AIAA JOURNAL
Vol. 42, No. 12, December 2004

Curvature Effect on Fracture Toughness of Cracked Cylindrical Shells Bonded with Patches

Xiannian Sun* and Liyong Tong†
University of Sydney, Sydney, New South Wales 2006, Australia

Adhesively bonded patch repair has been widely used as an efficient and economical method to extend the service life of cracked structural components. Most of the currently available analysis methods and empirical databases for composite bonded patch repair to flat structures are computationally efficient and easy to use. However, the current knowledge on composite bonded repair for flat structures cannot be directly applied to curved repairs. A novel adhesive element developed by the authors in conjunction with a shell element is employed to investigate the fracture toughness at the crack tip of a cracked cylindrical shell bonded with a composite patch. To validate the present finite element model for curved composite patch repairs, the stress intensity factors in a flat composite patch repair are first computed by the strain energy release rate analysis method and compared with those available in the literature. For the curved patch repairs, a full three-dimensional finite element analysis is also conducted to validate the proposed numerical model. Some selected numerical examples are given to demonstrate the effect of curvature on the fracture toughness of a cracked cylindrical shell bonded with a composite patch subjected to different types of loading.

I. Introduction

DAMAGE can occur in the form of a delamination or crack during manufacturing and/or service for most load-carrying structures. The challenging problem is how to repair these damaged structures to restore their original designated service life. The application of an adhesively bonded composite patch to repair a cracked thin-walled structure is widely used in aging aircraft because of its high structural efficiency and cost effectiveness.

A large amount of research work on designing and assessing composite repairs has been published since the early 1970s.[1–5] One of the most challenging aspects of composite bonded patch repair technology is to develop an accurate tool for investigating the fracture toughness of the cracked structures after repair. Because of the difficulty in producing an analytical solution for the composite bonded patch repair, most research work employs numerical methods to analyze the stress field at the crack tip, such as full three-dimensional finite element analysis (FEA),[6–8] two-dimensional FEA,[9,10] boundary element method,[11] etc. These currently available analysis methods and empirical databases are computationally efficient and easy to use for composite bonded patch repair to flat structures. However, curved thin-walled structures are also widely used in engineering applications, such as aircraft wing skin, fuselage, etc., and the current knowledge of composite bonded repairs for flat structures cannot be directly applied to those curved repairs. Therefore, it is necessary to study the curved repairs for better understanding of the effect of curvature on repair effectiveness.

The authors proposed a curved adhesive element formulation,[12] combined with a plate/shell element, to analyze the stress in the bond line of a curved bonded joint. In this paper, this adhesive element in conjunction with a serendipity degenerated shell element[13] is employed to investigate the effect of curvature on fracture toughness of the curved composite patch repairs. The stress intensity factors in a flat composite repair are first computed using the present finite element model and compared with those available in the literature. For the curved repairs, a full three-dimensional FEA is also conducted to validate the proposed numerical model. Finally, some selected numerical examples are given to demonstrate the effect of curvature on the fracture toughness of a cracked cylindrical shell bonded with a composite patch subjected to different types of loading.

Received 22 April 2003; revision received 7 June 2004; accepted for publication 10 June 2004.

*Research Associate, School of Aerospace, Mechanical and Mechatronic Engineering.
†Professor, School of Aerospace, Mechanical and Mechatronic Engineering. Senior Member AIAA.

II. Finite Element Model

Figure 1 shows a cylindrical metallic shell with an embedded through-thickness central crack, over which is bonded a single-sided composite patch. The overlap region can be modeled by the developed scheme,[12] in which both the shell and the patch are modeled using shell elements and the adhesive layer is modeled using pseudo-brick elements. The shell and patch are simulated using eight-noded serendipity degenerated shell elements considering transverse shear deformation, and the linear displacements are given by[13]

$$u(x, y, z) = u^0(x, y) + z\theta_y(x, y)$$

$$v(x, y, z) = v^0(x, y) - z\theta_x(x, y), \qquad w(x, y, z) = w(x, y) \tag{1}$$

where u, v, and w are the translational displacements and θ_x and θ_y are the rotations of the directional normal about x and y coordinate, respectively. The superscript zero denotes the midplane of the shell elements, which sandwiches the adhesive layer.

Accordingly, the adhesive layer is modeled by a 16-noded adhesive element.[12] The patch is assumed to be perfectly bonded to the curved surface with uniform thickness, and no debonding occurs in the entire adhesive layer. The thickness of adhesive layer is very thin compared to that of patch and curved surface. Therefore, the strains in the adhesive layer are assumed to be constant across the thickness of the adhesive layer. Only three out-of-plane stresses, σ_z, γ_{yz}, and γ_{xz}, are considered for the adhesive layer. Following these three assumptions, the three constant adhesive stains can be readily obtained as follows:

$$\varepsilon_{zz} = (1/t)(w_i - w_j)$$

$$\gamma_{yz} = (1/t)(v_{i'} - v_{j'}) = (1/t)\left[v_i^0 - v_j^0 + (H_u/2)\theta_{xi} + (H_l/2)\theta_{xj}\right]$$

$$\gamma_{xz} = (1/t)(u_{i'} - u_{j'}) = (1/t)\left[u_i^0 - u_j^0 - (H_u/2)\theta_{yi} - (H_l/2)\theta_{yj}\right] \tag{2}$$

where the subscripts i and j denote the corresponding upper and lower shell elements, respectively. H_u and H_l are the thickness of the upper and lower shell elements, namely, the thickness of the host shell and the bonded composite patch, respectively, and t is the thickness of the adhesive layer.

III. Fracture Toughness Analysis

A. Strain Energy Release Rate

In this paper, only mode 1 fracture loading is considered. The modified virtual crack closure technique[14] is employed to compute the mode 1 strain energy release rate. Note that the same procedure can also be used for mixed mode loading and for the computation of the mixed mode strain energy release rate (SERR).

Figure 2 shows a typical finite element mesh near the crack tip at point c, where the crack is assumed to be enclosed by a small length of Δa. The closure forces needed at points a and b are taken to be the same as those at points c and d, respectively. Thus, the SERR can be calculated as the work done by the nodal force (moment) F_{cy} and F_{dy} (M_{cx} and M_{dx}), in closing the crack opening displacement (rotation) v^0_{ay} and v^0_{by} (θ_{ax} and θ_{bx}). The total strain energy release rate is obtained as

$$G_t = G_u + G_b \tag{3}$$

where

$$G_u = 1/(2\Delta a \cdot H)\left[F_{cy}\left(v^0_{ay} - v^0_{a'y}\right) + F_{dy}\left(v^0_{by} - v^0_{b'y}\right)\right]$$

$$G_b = 1/(2\Delta a \cdot H)[M_{cx}(\theta_{ax} - \theta_{a'x}) + M_{dx}(\theta_{bx} - \theta_{b'x})] \tag{4}$$

where H is the thickness of the host shell, for example, H_u or H_l.

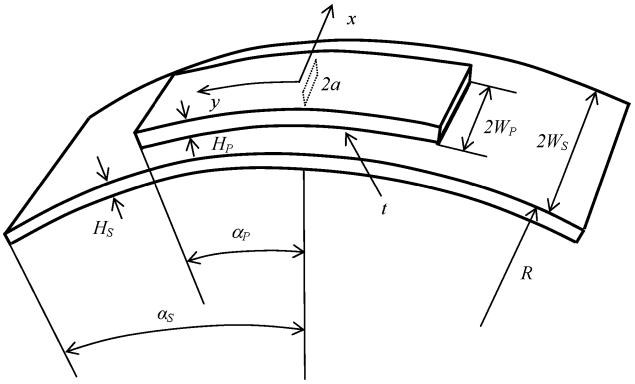

Fig. 1 Cracked cylindrical shell with bonded composite patch.

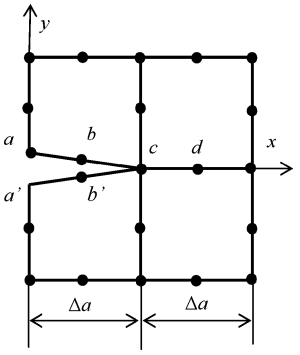

Fig. 2 Crack tip elements (top view).

B. Stress Intensity Factor

To compare the current analysis results with those in the literature, the SERR obtained from Eqs. (3) and (4) is transformed into stress intensity factor. According to Young and Sun,[15] if the rotational (bending) contribution to the strain energy release rate G_b is small, mode 1 stress intensity factor in the state of plane stress can be obtained by

$$K_l = K_u = \sqrt{G_u E_s} \tag{5}$$

where the subscript s denotes parameters associated with the host cylindrical shell.

If bending is not negligible, then stress intensity factor for pure bending moments in the state of plane stress can be given by

$$K_b = \sqrt{3G_b E_s} \tag{6}$$

Subsequently, the maximum stress intensity factor over the thickness of the plate is

$$K_l = K_u + K_b \tag{7}$$

IV. Numerical Verification

To verify the present finite element model for curved composite patch repairs, the stress intensity factors in the flat patch repairs and the SERRs in the curved patch repairs are computed and compared with those available in the literature and/or three-dimensional finite element solutions.

A. Single-Sided Composite Patch Bonded to Cracked Flat Plate

As shown in Fig. 3, a center-cracked aluminum plate, which is adhesively bonded with a boron composite patch on one side, has been investigated in previous studies.[8–10] The material properties and dimensions of the single-sided repair are given in Table 1 and are the same as those employed in previous studies. The total length of the central crack is $2a = 50.0$ mm. Because of the structural symmetry, only one-quarter of the single-sided repair is modeled.

The stress intensity factor is used to evaluate the fracture toughness at the crack tip with patch repairs to compare the results obtained by the present model with those available in the literature. Three load cases are considered in the calculation of the stress intensity factors by assuming that the local stress field near the crack tip is in a state of plane strain, which leads to the relationship between the SERR and the stress intensity factor as

$$K_l = \sqrt{GE/(1 - v^2)} \tag{8}$$

where v is Possion's ratio of the cylindrical shell.

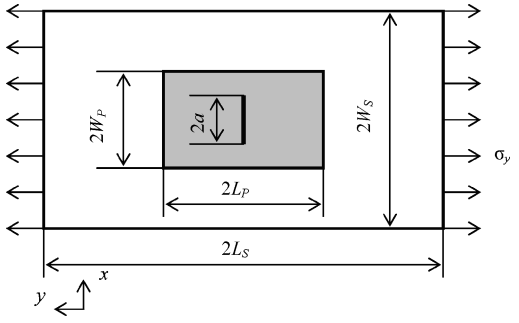

Fig. 3 Single-sided composite patch bonded to cracked flat plate.

Table 1 Material properties and dimensions of a single-sided flat repair

Layer	Length L, mm	Width W, mm	Thickness H, mm	Material properties
Aluminum plate	180.0	120.0	2.2900	$E = 71.02$ GPa, $v = 0.32$
Adhesive	76.0	38.0	0.1016	$E = 0.965$ GPa, $v = 0.32$
Composite patch	76.0	38.0	0.7620	$E_1 = 208$ GPa, $E_2 = E_3 = 25.44$ GPa $G_{23} = 4.94$ GPa, $G_{12} = G_{13} = 7.24$ GPa $v_{23} = 0.035$, $v_{12} = v_{13} = 0.1677$

Table 2 Comparison of K^m at the midplane for single-sided flat repair

	K^m				
λ	Present	Chue et al.[8] three dimensional	Sun et al.[9] two-dimensional plate model	Naboulsi and Mall[10] three-layer technique	Sun et al.[9] three dimensional
−2	0.555	0.392	0.493	0.552	0.565
0	0.607	0.481	0.536	0.570	0.612
2	0.658	0.571	0.579	0.609	0.660

Table 3 Comparison of K^f at the free surface for single-sided flat repair

	K^f				
λ	Present	Chue et al.[8] three dimensional	Sun et al.[9] two-dimensional plate model	Naboulsi and Mall[10] three-layer technique	Sun et al.[9] three dimensional
−2	0.992	0.742	0.900	0.945	0.933
0	1.050	0.902	0.953	0.982	0.985
2	1.108	1.062	1.007	1.019	1.036

Table 4 Material properties and dimensions of a single-sided curved repair

Layer	Sector angle α, mm	Width W, mm	Thickness H, mm	Material properties[a]
Aluminum shell	30.0	30.0	1.0	$E = 70.0$ GPa, $v = 0.30$
Adhesive	15.0	15.0	0.15	$E = 2.4$ GPa, $v = 0.30$
Composite patch	15.0	15.0	1.0	$E_1 = 208$ GPa, $E_2 = E_3 = 25.44$ GPa $G_{23} = 4.94$ GPa, $G_{12} = G_{13} = 7.24$ GPa $v_{23} = 0.035$, $v_{12} = v_{13} = 0.1677$

[a]Radius of the outer surface of the shell is $R = 100.0$ mm.

The three load cases are $\lambda = -2$, $\lambda = 0$, and $\lambda = 2$, where the biaxial load factor λ is defined as

$$\lambda = \sigma_x/\sigma_y \tag{9}$$

The stress intensity factors are normalized with respect to $\sigma_y\sqrt{(\pi a)}$, that is, the normalized value for the stress intensity factor is

$$K = K_I \Big/ \sigma_y\sqrt{\pi a} \tag{10}$$

This problem has been investigated by Chue et al.[8] and Sun et al.,[9] using three-dimensional FEA and also by Sun et al.[9] and Naboulsi and Mall[10] using Mindlin plate theory and the three-layer technique, respectively. The three-dimensional finite element solutions show that the stress intensity factor through the plate thickness is nearly linear, which supports the use of plate/shell elements that assume a linear distribution of bending stress over the plate thickness.[9] Therefore, comparisons of the single-sided composite repairs stress intensity factor are made at the plate midplane and free edge. Tables 2 and 3 list the normalized stress intensity factors at the midplane, K^m, and at the free surface of the plate, K^f.

The three-dimensional finite element solutions in Refs. 8 and 9 are obtained using two and more layers of 20-noded brick elements across the aluminum plate thickness and later the model is refined. The present stress intensity factors at both the midplane and the free surface are in a very good agreement with those from the Sun et al. three-dimensional model,[9] especially for the results at the midplane with the difference being less than 2%. For the stress intensity factors at the free surface, the maximum difference is 7%. Furthermore, the present results at the midplane are in better agreement with three-dimensional finite element solutions than those from Mindlin plate theory (see Ref. 9) and the three layer technique[10] because of the use of a more accurate eight-node element, whereas four-node elements are used in the latter two analyses. This clearly shows the validity and advantage of the present finite element model in the analysis of flat composite patch repair.

B. Single-Sided Composite Patch Bonded to Cracked Cylindrical Shell

As shown in Fig. 1, a center-cracked cylindrical shell, which is adhesively bonded with a boron composite patch at its outer surface, is considered. The material properties and dimensions of the single-sided curved repair are given in Table 4. The total length of the central crack is $2a = 15.0$ mm. Only one-quarter of the single-sided repair is modeled due to the structural symmetry. The three biaxial load cases are $\lambda = -2$, $\lambda = 0$, and $\lambda = 2$ with $\sigma_y = 1.0$ MPa, where λ is defined in Sec. IV.A.

Table 5 Comparison of G_t for single-sided curved repair

λ	Present G_t, J/m^2	Three dimensional G_{t0}, J/m^2	$(G_t - G_{t0})/G_{t0}$, %
−2	41.89	40.64	3.1
0	41.52	39.98	3.8
2	41.15	39.33	4.6

For the curved structure, the SERR is widely used to evaluate the fracture toughness instead of stress intensity factor. Therefore, the SERR is employed to assess the curvature effect on the fracture toughness of the curved composite patch repairs. Table 5 lists the total strain energy release rate obtained using three-dimensional finite element analysis and the present finite element model.

A commercial FEA software, STRAND7,[16] is used to conduct a three-dimensional FEA of a curved composite patch repair. For the three-dimensional finite element model, nine layers and two layers of eight-node brick elements are employed for the cylindrical shell and the bonded patch, respectively. As a convergence analysis, one, two, and four layers of brick element are used for the adhesive layer, which shows that one layer of brick elements can provide enough accuracy for the fracture toughness analysis. This is also testified in Ref. 6 for the stress intensity factor in the flat patch repairs. The results in Table 5 are obtained by four layers of brick elements in the adhesive layer (14,388 nodes and 43,164 degrees of freedom for three-dimensional model vs 4521 nodes and 27,126 degrees of freedom for the present shell element model).

From Table 5, it can be seen that the total SERRs obtained by the present shell element model correlate well to those calculated by the three-dimensional finite element model with the maximum relative difference less than 5%. A possible reason that may contribute to the difference in the SERR between the three-dimensional and present finite element models is the difference in the simulation of the adhesive layer. Only three out-of-plane stresses in the adhesive layer are considered in the present model, whereas all six stress components are taken into account in the three-dimensional

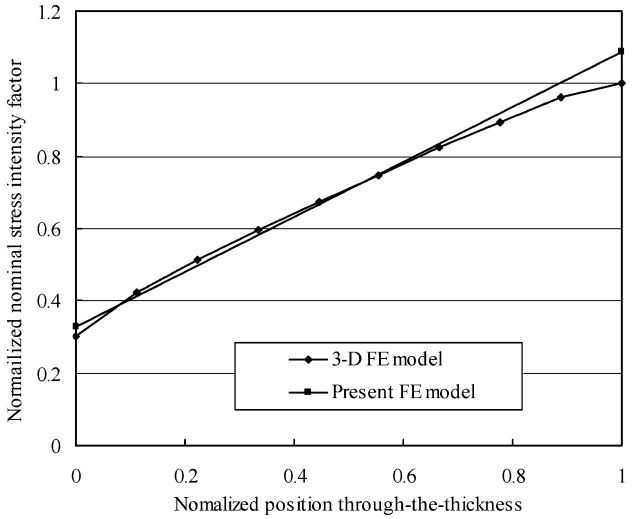

Fig. 4 Distribution of normalized stress intensity factor though-the-thickness of cylindrical shell ($\lambda = 0$) for single-sided repair.

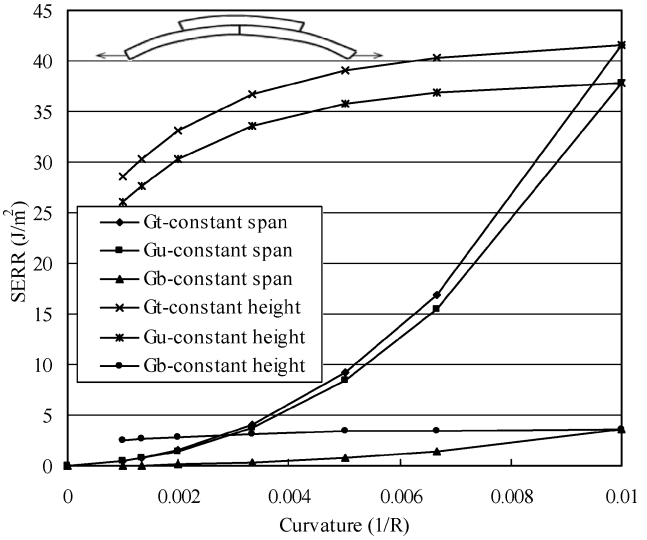

Fig. 5 SERRs of single-sided curved composite patch repairs subjected to tensile loads.

finite element model. On the other hand, crack closure in regions of compression at the crack tip is not considered in the present model. Although the crack closure is not found for the present numerical examples in the three-dimensional FEA, note that ignoring the crack closure may produce some errors when the structure undergoes a large deformation or is subjected to a large bending moment.

To further compare the fracture toughness results predicted by the present shell model with those of the three-dimensional finite element model, a nominal stress intensity factor is calculated using the formulas in Sec. IV.A. Note that the nominal stress intensity factor used here is for comparing the energy distribution through-the-thickness of cylindrical shells at the crack tip predicted by both models. According to Eq. (7), the nominal stress intensity factor is assumed to be linearly distributed through the cylindrical shell thickness in the present shell model. The three-dimensional FEA shows that this distribution is almost linear, which is shown in Fig. 4 with the origin measured from the adhesive–shell interface. It can be seen in Fig. 4 that the nominal stress intensity factor distributions calculated by both models agree well with each other.

The numerical results given in Table 5 and Fig. 4 indicate that the present shell model can effectively and efficiently be used to predict the influence of bonded patch on the fracture toughness of a cracked shell structure.

V. Numerical Results and Discussion

A. Single-Sided Curved Composite Patch Repairs Subjected to Tensile Loads

Consider the same configuration of curved bonded repair as that in Sec. IV.B. Only tensile loads in the y direction, $\sigma_y = 1.0$ MPa, are applied to both ends of the cylindrical shell. Two cases are analyzed, that is, keeping the span ($R \sin\alpha_S = 50.0$ mm) or the height [$R(1 - \cos\alpha_S) = 13.4$ mm] of the cylindrical shell constant, respectively. The constant length of the bonded patch is 26.18 mm. The crack length is $2a = 15.0$ mm. All other structural dimensions and material properties are the same as those described in Sec. IV.B.

Figure 5 shows the strain energy release rates for different radius of cylindrical shell and for both cases. When the height of the cylindrical shell is kept constant, both the bending moment M_x and membrane force F_y are nearly constant at the crack plane. It can be seen from Fig. 5 that the total SERR increases with curvature, $1/R$, whereas the comparison of the closure and rotational contributions to the total SERR indicates that a larger curvature can result in a marginal increase in the pure bending SERR G_b and a significant increase in the closure contribution to the SERR, G_u. When the span of the cylindrical shell is kept constant, only the membrane force F_y is constant at the crack plane, whereas the bending moment at

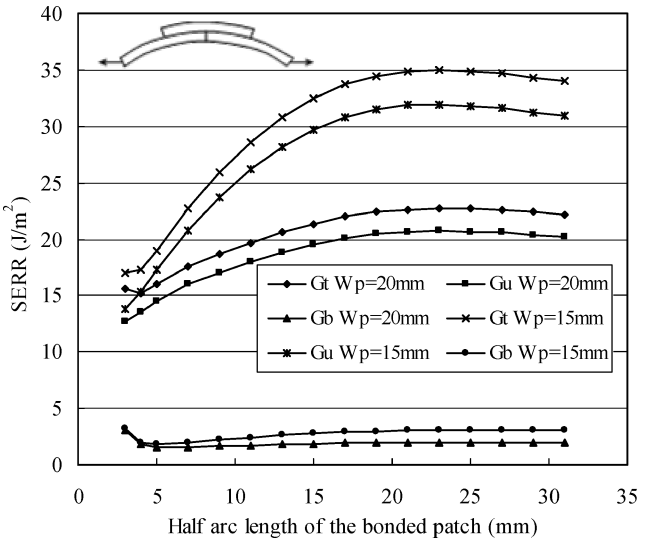

a) R = 100 mm

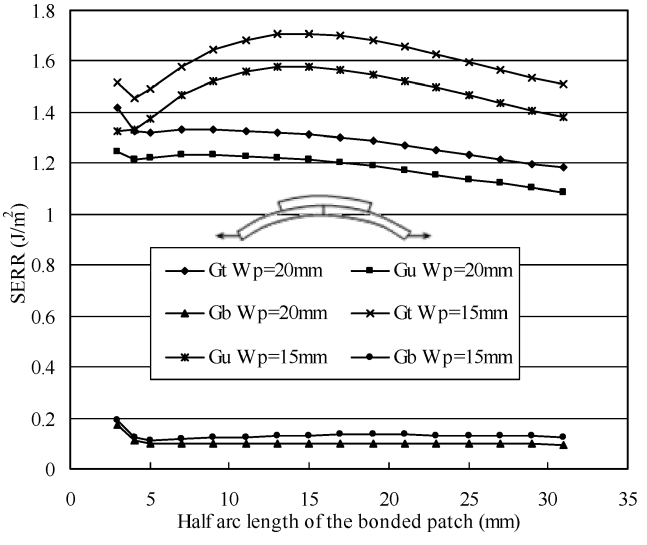

b) R = 500 mm

Fig. 6 Patch size effect on SERR of single-sided curved composite patch repairs subjected to tensile loads.

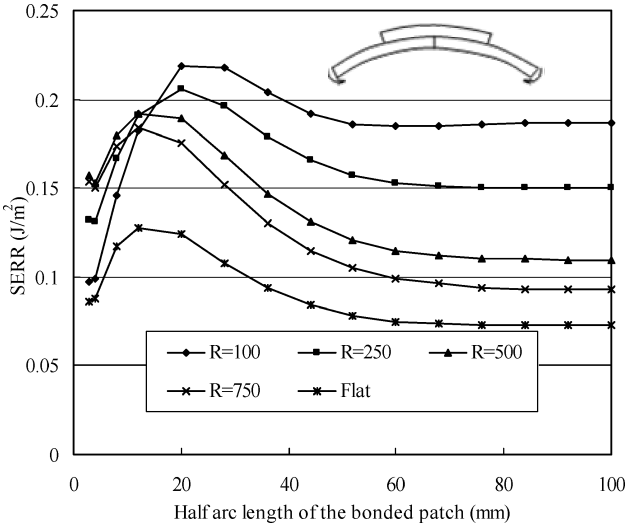

a) G_t (W_P = 15 mm)

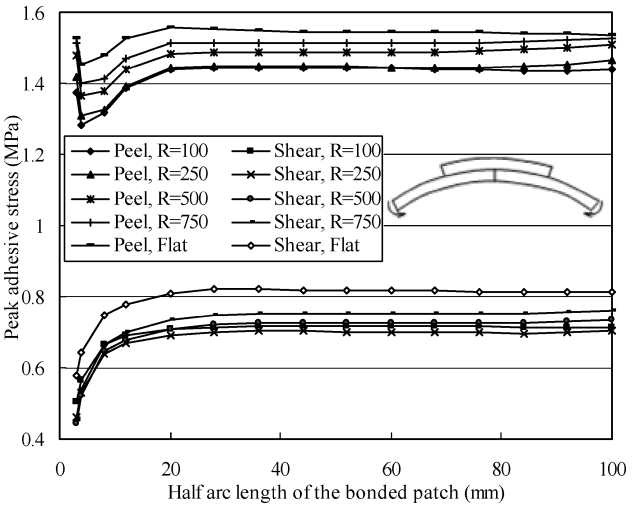

d) Peak adhesive stresses in middle line of bonded patch (W_P = 15 mm)

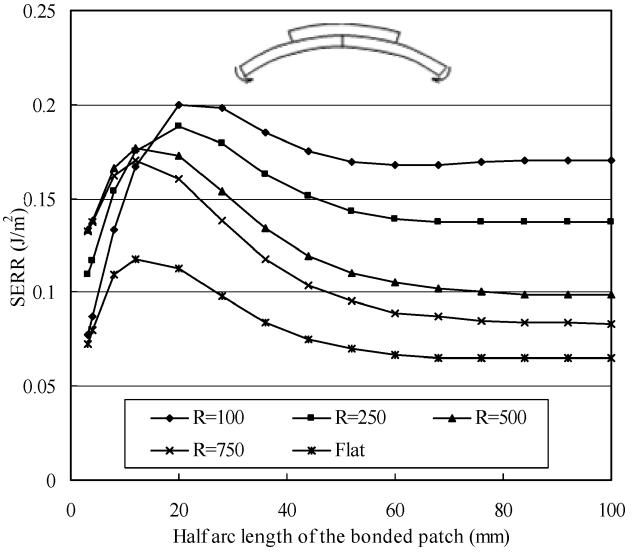

b) G_u (W_P = 15 mm)

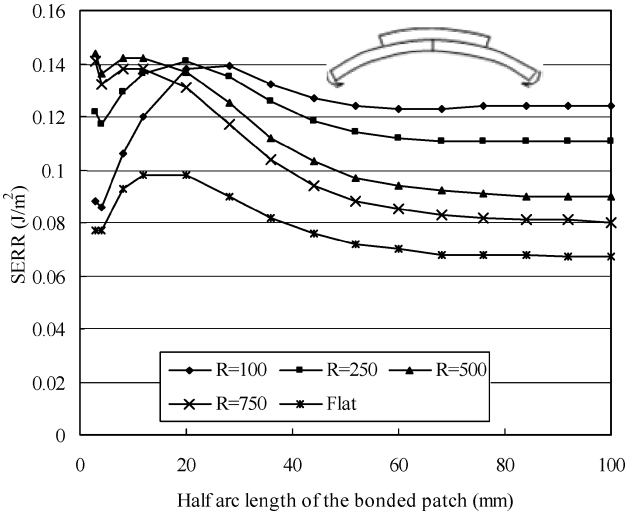

e) G_t (W_P = 20 mm)

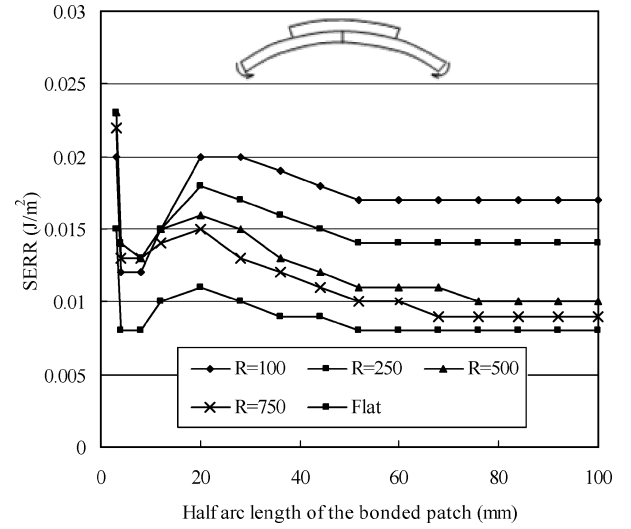

c) G_b (W_P = 15 mm)

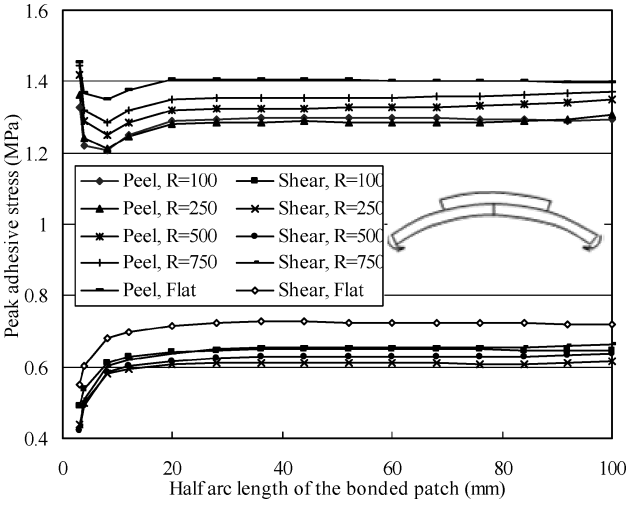

f) Peak adhesive stresses in middle line of bonded patch (W_P = 20 mm)

Fig. 7 Stress intensity factors and peak adhesive stresses in single-sided curved composite patch repairs subjected to bending moments.

the crack plane will increase for the larger curvature. From Fig. 5, it is evident that the larger bending moment at the crack plane can lead not only to a significant increase in G_u, but also a considerable increase in G_b. Consequently, it results in a substantial increase in the total SERR.

To investigate the effect of patch size on the SERR of curved patch repairs subjected to tensile loads, the host cylindrical shell is kept unchanged, while the arc length and the width of the bonded composite patch is varied. The host shell is assumed to have a width $W_s = 30$ mm and half arc length of 50 mm. Two values of radius are considered, that is, $R = 100$ mm and $R = 500$ mm. Two cases of patch width are computed, $W_p = 15$ mm and $W_p = 20$ mm. The crack length is assumed to be $2a = 15$ mm. The thickness and material properties for the host metallic shell, bonded composite patch, and adhesive layer are the same as those described in Sec. IV.B. A tensile load, $\sigma_y = 1.0$ MPa, is applied.

Figure 6 shows the SERR vs patch size. From Fig. 6, when the arc length of the bonded patch is very short, that is, half arc length is 3.0–4.0 mm, the total SERR G_t and the rotational SERR G_b decrease rapidly from the much higher values of the unpatched cracked shell, which are not shown. The closure SERR G_u, however, varies slightly with different radii and widths of the bonded patch. Further investigation into the adhesive stresses shows that much higher peak peel stress and lower peak shear stress occur on both free ends of the adhesive layer and in the middle of the adhesive layer where the crack face is located. It indicates that the adhesive layer is not long enough to transfer the applied loads into the bonded patch. However, the extension of arc length of the bonded patch, as shown in Fig. 6, leads to an increase in the SERR and follows a slow decrease again with a longer bonded patch. For a smaller radius of the cylindrical shell, $R = 100$ mm, the increase in the total SERR is more significant than for a larger radius, $R = 500$ m, and is 106 and 18% for $W_p = 15$ mm, respectively. A comparison of G_t for different widths of the bonded patch shows that a wider patch can result in lower strain energy release rate.

B. Single-Sided Curved Composite Patch Repairs Subjected to Bending Moments

To further identify the effect of curvature on fracture toughness of the curved patch repair, a composite patch repair subject to a constant bending moment is considered. As shown in Fig. 1, the arc length of the cylindrical shell is kept constant at 150.0 mm. A pair of uniform bending moments about the x axis, $m_x = 1.0$ KN, is applied to both ends of the bonded repair. The crack length is $2a = 15.0$ mm. The radius of the curved repairs, the arc length, and the width of the bonded patch are given in Fig. 7. For the flat repairs, patch length equals the arc length of the curved repairs. The other structure dimensions and the material properties are the same as those described in Sec. IV.B.

Figure 7 shows the SERRs and the peak adhesive stress at the free end of the bond line ($x = 0$ and $y = -W_p$) for different radii of cylindrical shell bonded with different sizes of patches. Similar to the case of tensile loads, G_t and G_b drop to a very low level with a very short arc length of the bonded patch, whereas G_u increases, as shown in Figs. 7a–7c and 7e. Further extension of the arc length of the bonded patch leads to an increase of the SERRs (G_t, G_u, and G_b). After the SERRs achieve their asymptotic values simultaneously, the SERRs decrease with the prolonged arc length of the bonded patch. On the other hand, the peak value of the peel stress (as shown in Figs. 7d and 7f) in the adhesive layer decreases first with a very short arc length of the bonded patch and then increases slightly to its asymptotic value and tends to be steady for any further extension of the arc length of bonded patch. The peak value of adhesive shear stress, however, increases monotonously to its asymptotic value with a very short arc length of the bonded patch and then tends to be steady.

A comparison of SERR for different radii of the bonded patch repairs subjected to a pair of bending moment shows that a larger curvature $(1/R)$, that is, smaller radius of the patch repairs, leads to a higher value of SERR after the SERRs achieve their asymptotic values, whereas the peak values of the adhesive stresses at $x = 0$, $y = -W_p$ decrease for larger curvature of the patch repairs. This trend is more clearly shown in Fig. 8 with half the arc length and half the width of the bonded patch 20 and 15 mm, respectively. Note from Fig. 8 that G_t, G_u, and G_b are increased by 95.6, 95.2, and 81.8%, respectively, when the curvature of the cylindrical shell varies from 0 (flat) to 0.01. This difference indicates that the effect of curvature tends to result in higher SERR at the crack tip with an increase in the curvature of curved repairs with longer bonded patch subjected to the bending moment. However, the medium radius of curved repairs seems to have a higher value of SERR when the arc length of the bonded patch is shorter. For example, the highest value of G_t is obtained when $R = 500$ mm with the arc length of the bonded patch in the range of 3–12 mm, as shown in Figs. 7a and 7e.

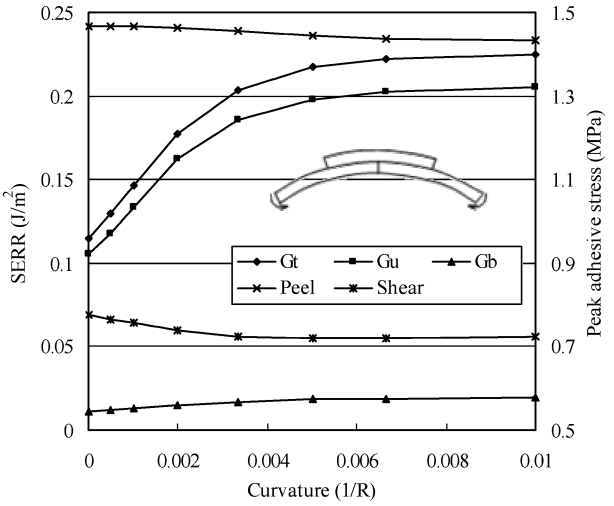

Fig. 8 Curvature effect on SERR of single-sided curved composite patch repairs subjected to bending moments (half constant arc length of the bonded patch 20 mm).

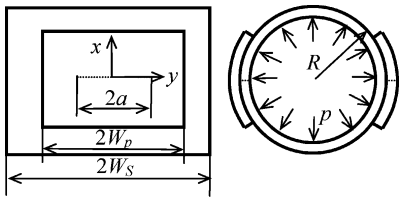

Fig. 9 Through-thickness cracked circular cylindrical shell bonded with two composite patches subjected to internal pressure.

From Fig. 7, note that an increase in the width of the bonded patch leads to a lower value of the SERR and a lower peak value of the adhesive stresses. Therefore, it is recommended to increase the width of the bonded patch for diminishing the SERR and the adhesive stresses.

C. Single-Sided Curved Composite Patch Repairs Subjected to Internal Pressure

Figure 9 shows a circular cylindrical shell in which are embedded two symmetric through-thickness cracks, repaired by bonding with two external patches that are located symmetrically about the vertical line passing through the center of the shell. The circumferential and longitudinal coordinate x and y are measured from the center of the bonded patch. The cylindrical shell has a width $2W_s = 100$ mm, a radius R, and the length of the symmetric through-thickness crack is $2a = 15$ mm. The bonded patch has a width $2W_p = 40$ mm. The thickness and material properties for the host shell, the adhesive layer, and the bonded patch are the same as in Sec. IV.B. The cylindrical shell is assumed to be subjected to an internal pressure. The longitudinal displacement at both ends of the cylindrical shell is assumed be fixed. Only a quarter of the structure is taken for analysis due to its symmetry.

To identify clearly the effect of curvature on the SERR for the curved patch repairs subjected to an internal pressure, the circumferential stress in the undamaged host cylindrical shell is kept constant.

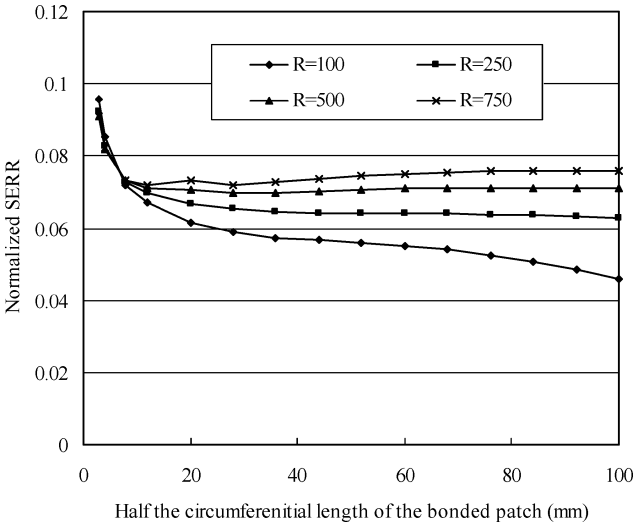

Fig. 10 Curvature effect on total SERR of cracked circular cylindrical shell bonded with two external composite patches subjected to internal pressure.

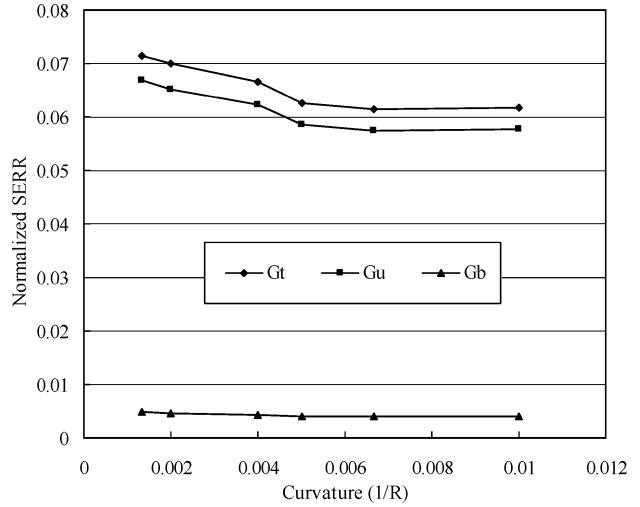

Fig. 11 Curvature effect on the SERR of cracked circular cylindrical shell bonded with two external composite patches subjected to internal pressure (constant sector angle of the bonded patch is 0.4 rad).

Because of the high ratio of thickness-to-radius of the cylindrical shell, the circumferential stress can be approximately given by

$$\sigma_\theta = (R/H_S)p \tag{11}$$

where H_S is the thickness of the host cylindrical shell.

Then the strain energy release rate is normalized by

$$\bar{G} = G/\sigma_\theta \tag{12}$$

Figure 10 shows the curves of the SERR vs the circumferential length of the bonded patch for different radii of the host cylindrical shell. Note that the total SERR remarkably decreases with the circumferential length of the bonded patch. However, further extension of the circumferential length of the bonded patch can only reduce the total SERR for the cylindrical shell with a large curvature, such as $R = 100$ mm. For other two cases, $R = 250$ and 500 mm, the total SERR tends to remain unchanged with longer circumferential length of the bonded patch. For $R = 750$ mm, an increase in circumferential length of the bonded patch seems to lead to a slight increase in the total SERR. On the other hand, a comparison of the total SERR for different radii of host shells with the same circumferential length of the bonded patch shows that larger curvature (smaller radius) results in a lower total SERR. Further investigation into the total SERR for different radii of the host shell with the same sector angle of the bonded patch, as shown in Fig. 11, shows that an increase of curvature can lead to a slight decrease in the total SERR.

VI. Conclusions

A finite element model is proposed to investigate the fracture toughness of the cracked cylindrical shell repaired by a single-sided bonded composite patch. The present model is validated by comparing the predicted stress intensity factors at the midplane and free surface with those results available in the literature for flat repairs. The total SERRs at the crack tip predicted by the present model are slightly higher than those obtained by three-dimensional FEA. The selected parametric study results show that the effect of curvature on the SERR can be significant and is dependent of geometrical configuration, applied loading, and boundary condition of the host structures bonded with curved patch repairs.

Acknowledgments

The authors are grateful for the support of the Asian Offices of Aerospace Research and Development/Air Force Office of Scientific Research (AOARD/AFOSR). The authors acknowledge valuable technical discussions with and encouragement from N. Pagano and G. Schoeppner of the U.S. Air Force Research Laboratory, O. Ochoa of AFOSR, and M. Nowak and T. Kim of AOARD/AFOSR.

References

[1]Baker, A. A., "Repair of Cracked or Defected Metallic Aircraft Components with Advanced Fibre Composites—An Overview of Australian Work," *Composite Structures*, Vol. 2, No. 2, 1984, pp. 153–181.

[2]Baker, A. A., and Jones, R., *Bonded Repair of Aircraft Structures*, Martinus Nijhoff, Dordrecht, The Netherlands, 1988.

[3]Hart-Smith, L. J., "The Design of Repairable Advanced Composite Structures," Douglas Aircraft Co., Douglas Paper 7550, McDonnell Douglas, Denver, CO, June 1985.

[4]Adams, R. D., Comyn, J., and Wake, W. C., *Structural Adhesive Joints in Engineering*, 2nd ed., Chapman and Hall, London, 1997.

[5]Tong, L., and Steven, G. P., *Analysis and Design of Structural Bonded Joints*, Kluwer Academic, Boston, 1999.

[6]Umamaheswar, T. V. R. S., and Singh, R., "Modeling of a Patch Repair to a Thin Cracked Sheet," *Engineering Fracture Mechanics*, Vol. 62, No. 2, 1999, pp. 267–289.

[7]Bouiadjra, B. B., Belhouari, M., and Serier, B., "Computation of the Stress Intensity Factors for Repaired Cracks with Bonded Composite Patch in Mode I and Mixed Mode," *Composite Structures*, Vol. 56, No. 4, 2002, pp. 401–406.

[8]Chue, C. H., Chang, L. C., and Tsai, J. S., "Bonded Repair of a Plate with Inclined Central Crack Under Biaxial Loading," *Composite Structures*, Vol. 28, No. 1, 1994, pp. 39–45.

[9]Sun, C. T., Klug, J., and Arendt, C., "Analysis of Cracked Plates Repaired with Bonded Composite Patches," *AIAA Journal*, Vol. 34, No. 2, 1996, pp. 369–374.

[10]Naboulsi, S., and Mall, S., "Modeling of a Cracked Metallic Structure with Bonded Composite Patch Using the Three Layer Technique," *Composite Structures*, Vol. 35, No. 3, 1996, pp. 295–308.

[11]Young, A., Rooke, D. P., and Cartwright, D. J., "Analysis of Patched and Stiffened Cracked Panels Using the Boundary Element Method," *International Journal of Solid Structures*, Vol. 29, No. 17, 1992, pp. 2201–2216.

[12]Tong, L., and Sun, X., "Adhesive Elements for Stress Analysis of Bonded Patch to Curved Thin-Walled Structures," *Computational Mechanics*, Vol. 30, No. 2, 2003, pp. 143–154.

[13]Zienkiewicz, O. C., and Taylor, R. L., *The Finite Element Method*, 4th ed., Vol. 1, Basic Formulation and Linear Problems, McGraw–Hill, London, 1989.

[14]Rybicki, E. F., and Kanninen, M. F., "A Finite Element Calculation of Stress Intensity Factors by a Modified Crack Closure Integral," *Engineering Fracture Mechanics*, Vol. 9, 1977, No. 4, pp. 931–938.

[15]Young, M. J., and Sun, C. T., "On the Stain Energy Release Rate for a Cracked Plate Subjected to Out-of-Plane Bending Moment," *International Journal of Fracture*, Vol. 60, No. 3, 1993, pp. 227–247.

[16]"Using Strand 7—Introduction to the Strand7 Finite Element Analysis System," ed. 1, G+D Computing Pty, Ltd., Sydney, Australia, May 1999.

K. Shivakumar
Associate Editor